Title

The Making and Breaking of Lead-Free Double Perovskite Nanocrystals of Cesium Silver—Bismuth Halide Compositions

Journal

Nano Letters, 18(6)

ISSN

1530-6984

Authors

Bekenstein, Yehonadav
Dahl, Jakob C
Huang, Jianmei
et al.

Publication Date

2018-06-13

DOI

10.1021/acs.nanolett.8b00560

Peer reviewed

The Making and Breaking of Lead-Free Double Perovskite Nanocrystals of Cesium Silver-Bismuth Halide Compositions

Yehonadav Bekenstein,[1,3] Jakob C. Dahl,[1,3,4] Jianmei Huang[1], Wojciech T. Osowiecki[1,3], Joseph K. Swabeck[1,3], Emory M. Chan[4], Peidong Yang,[1,2,3,5] and A. Paul Alivisatos,[1,2,3,5]

[1]Department of Chemistry and [2]Department of Materials Science and Engineering, University of California, Berkeley, CA 94720, United States

[3]Materials Sciences Division and [4]Molecular Foundry, Lawrence Berkeley National Laboratory, Berkeley, CA 94720, United States

[5] Kavli Energy NanoScience Institute, Berkeley, CA 94720, United States

KEYWORDS: lead-free halide perovskites, double perovskites, cesium silver bismuth halides, perovskite nanocrystals

ABSTRACT: Replacing lead in halide perovskites is of great interest due to concerns about stability and toxicity. Recently, lead free double perovskites

in which the unit cell is doubled and two divalent lead cations are substituted by a combination of mono- and trivalent cations have been synthesized as bulk single crystals and as thin films. Here, we study stability and optical properties of all-inorganic cesium silver (I) bismuth (III) chloride and bromide nanocrystals with the double perovskite crystal structure. The cube shaped nanocrystals are monodisperse in size with typical side lengths of 8 to 15 nm. The absorption spectrum of the nanocrystals presents a sharp peak, which we assign to a direct bismuth s-p transition and not to a quantum confined excitonic transition. Using this spectroscopic handle combined with high resolution transmission electron microscopy (TEM) based elemental analysis, we conduct stoichiometric studies at the single nanocrystal level as well as decomposition assays in solution and observe that Ag^{+} diffusion and coalescence is one of the pathways by which this material degrades. Drying the nanocrystals leads to self-assembly into ordered nanocrystal solids, and these exhibit less degradation than nanocrystals in solution. Our results demonstrate that Cs_2AgBiX_6 (X = Cl, Br) nanocrystals are a useful model system to study structure-function relationships in the search for stable non-toxic halide perovskites.

TEXT

Interest in lead halide perovskite in recent years has grown rapidly following early observations of high efficiencies in optoelectronic applications that challenge our understanding of these materials.[1–3] Following

the surprising observations of good photovoltaic conversion efficiency, potential applications for lead halide perovskites have expanded to include color-tunable light emitting devices, optically pumped low threshold lasers and efficient photodetectors.[4-6]

In practice, the viability and use of lead halide perovskites in large scale manufacturing is currently limited by two main concerns: the toxicity of lead and the materials low stability to common operating conditions such as moisture and heat.[7,8]

To circumvent this problem, stable and lead free perovskite systems are a current focus of research in new materials chemistry. Several chemical design rules can serve as guides to this overall search: Structurally, Goldschmidt factors[9] and cation/anion radius ratios[10] can help suggest where to look for stable perovskite phases.[11] Electronic applications require materials that exhibit a direct band gap and strongly allowed lowest optical transition that support efficient absorption and emission processes desirable for optoelectronic devices. This electronic and orbital symmetry consideration appears at least to largely restrict the search to the p-block metals Sn, Pb, In, Tl, Sb and Bi with an allowed s-p band gap transition.

By substituting Pb^{2+} with Sn^{2+}, one can make the analogous Sn^{2+} based perovskite system that exhibits a direct bandgap transition and already has resulted in devices yielding 6% power conversion efficiencies.[12,13] Unfortunately, the thermodynamically favored Sn^{4+} makes

oxidation a major stability challenge for tin based perovskites and devices.[14,15] Other nontoxic divalent cations with appropriate optical transitions and a compatible ionic radius are challenging to find. Cations that deviate significantly from the octahedral and Goldschmidt tolerance constraints may result in zero, one and two dimensional perovskite derivatives which may demonstrate lower charge mobility and less favorable optoelectronic properties.[16–18]

Recently, the concept of a heterovalent substitution, in which the unit cell is doubled and a pair of Pb(II) ions is replaced by one M(I) cation and one M(III) cation, was demonstrated with the successful replacement of Pb(II) with Ag(I) and Bi(III) (Scheme in Figure 1a). The resulting $Cs_2AgBiBr_6$ material is significantly more heat and moisture resistant than most metal halide perovskites, however the reported electronic structure for this material shows an indirect bandgap transition.[19–21] Since the initial reports of these materials, most efforts have focused on predicting and synthesizing alternate compositions of double perovskites[22,23]and investigating possibilities of doping that favor direct electronic transitions.[24–26]

Synthesis of Cs_2AgBiX_6 (X = Cl, Br) double perovskite nanocrystals have been reported recently.[27] Nanocrystals are interesting as single structural domains where chemical transformations and finite size electronic effects can be studied. In this work we further investigate the optical properties and stability of the double perovskite nanocrystals (NCs). We have synthesized

nanocrystals with edge lengths of 8-15 nm and studied the structure and enhanced optical properties of this new family of nanocrystals. Although we did not observe significant quantum confinement in these materials, we elucidated several key parameters that influence their stability and valuable to the further development of stable, lead-free double perovskites.

We have succeeded in identifying two possible synthetic routes towards silver-bismuth double perovskite nanocrystals. In designing the synthesis we implemented knowledge from the recent success of $CsPbX_3$ (X = Cl, Br, I) colloidal nanocrystal synthesis. For the synthesis of nanocrystals, a solution of AgBr and $BiBr_3$ in octadecene with oleylamine and oleic acid was injected with Cs-Oleate at elevated temperatures (150-200 °C), in a procedure modified from the $CsPbX_3$ nanocube synthesis of Protescesu et al. [28]. A second synthetic procedure derived from a $CsPbCl_3$ synthesis developed by Xu et al.[29] uses lower growth temperatures (100 °C) and injection of halide precursor into a solution of metal acetates. Both procedures yield similar nanocrystals (Figure S2). For the chloride composition, we were able to use aqueous hydrochloric acid to synthesize small, high-quality nanocrystals, whereas hydrobromic acid did not yield a clean product for the $Cs_2AgBiBr_6$ composition, leading us to use trimethylsilylbromide. The ionic nature of the metathesis reaction dictates the rapid nucleation and growth kinetics of the resulting nanocrystals. As a result the reaction time plays almost no role in determining the resulting NC sizes and most of the reaction is completed after 40 seconds, analogous to the reaction time of colloidal lead halide

nanocrystals. Longer growth times lead to only small increases in size (Figure S3). In our typical synthesis, NCs present as highly crystalline with cubic shape of 8-15 nm side length and ~15% size distribution (Figure 1b,c and S4 and S5).

X-ray diffraction patterns measured on the NCs (Figure 2a) match those of reported $Cs_2AgBiBr_6$ and $Cs_2AgBiCl_6$ bulk materials, with the exception of broadened peaks that are expected due to the finite size of the nanocrystals. Scherrer analysis estimates sizes of 12±1 nm, and 5±1 nm for the Br and Cl compositions respectively (Figure S6), in agreement with TEM statistics. XRD analysis also reveals that the NCs are of the cubic structure with a Fm-3m space group and lattice spacing of 11.2 Å, roughly double that of the cubic lead halide perovskites. Single NC high resolution transmission electron microscopy (HRTEM) studies, show similar lattice spacing of 11.1 Å (figure 2c,d), these studies also confirm the crystals are bounded by <001> surfaces. In most cases, this zone axis is closely aligned with the TEM optical axis due to the cubic morphology of the crystals. These properties simplify structural studies at the atomic level. For example, three types of atomic columns exist parallel to the <001> axis: Br columns, Cs columns and mixed Ag,Bi,Br columns. Indeed the HRTEM demonstrated columns of different contrast similar to those depicted in the cartoon (Figure 2c).

The ability to make high quality, size controlled, colloidal double perovskite nanoparticles allows us to systematically investigate their optical properties, which we hypothesized to be different from bulk. To the naked

eye, the $Cs_2AgBiBr_6$ NC suspension with its distinct yellow color is clearly optically different from the orange-red color of bulk material (Figure 3a, inset). Dilute solutions of $Cs_2AgBiBr_6$ NCs have a typical absorption spectrum featuring a sharp absorption peak positioned at ~430 nm and a long absorption tail at longer wavelengths, suggesting an indirect transition consistent with the reported bulk properties. A similar functional form with a sharp peak is observed for the Cl compositions, with the peak positioned at 365 nm (Figure 3a). The Br compositions exhibit detectable photoluminescence centered around 650 nm, with a full width half maximum of ~200 nm. The weak and broad emission is further consistent with an indirect transition or trap emission, similar to the emission reported for bulk. In the case of the Cl compositions no detectable emission was measured at room temperature. To further demonstrate the relationship of absorption and emission spectra, photoluminescence excitation spectra (PLE) were acquired at the 650 nm emission line. The resulting spectrum coincides with the absorption peak at 430 nm, further verifying that light absorbed at the 430 nm peak, is emitted from the nanocrystals. . (Figure 3b red curve). A Tauc analysis of a diffuse reflectance measurement of a nanocrystal powder, assuming an indirect allowed transition is shown in Figure 3c and discussed in the SI. The linear regions are assigned to a phonon-assisted absorption process and transitions at 1.85eV and 2.09eV and a bandgap value of 1.97eV which is similar to the bulk material.[17] The absorption peak at 430 nm, which is the prominent optical feature for the $Cs_2AgBiBr_6$ NCs, is intriguing. This

peak is centered at 2.88eV, more than 1eV blue shifted from the band edge. It was not discussed in the initial studies of the bulk material and superficially suggests quantum confinement of an exciton.[17] A confinement energy as large as 1eV may occur and was reported for quantum confined perovskite nanoplates.[30–32] However, it is expected to be strongly dependent on the size and dielectric environment confining the exciton. To test for this dependence we intentionally varied the NC synthetic conditions. We used different precursors, temperatures and ligands that changed both the size and dielectric environment of the NCs. A size series of the NCs is presented in figure 3d. The position of the absorption did not significantly shift, demonstrating that the peak does not in fact originate from a confined exciton. Recent work that measured absorption via transmission measurement, instead of diffuse reflectance verified this peak also exists in thin $Cs_2AgBiBr_6$ bulk materials, further supporting the above argument.[33]

To further understand the functional shape of the absorption spectra beyond an excitonic contribution we turned to spectrographic studies of bismuth halides and ternary materials that contain bismuth and halides.[34,35] Isolated metal halide molecular complexes containing filled s^2 orbitals were spectroscopically studied by Oldenburg and Vogler, showing metal-centered s-p transitions, which resemble absorption features of halide perovskites.[36] For example, an isolated octahedral $BiBr_6^{3-}$ complex has a sharp absorption peak at 380 nm and no emission. In $Cs_2AgBiBr_6$ crystals, the connected BiBr octahedra are embedded into a larger dielectric constant material, (51 in

$Cs_2AgBiBr_6$[37] vs 37 in acetonitrile [36]) that can qualitatively account for the observed red shifted 6s-6p transitions (430 nm absorption peak).

Heightened interest in these materials is due to their practical application as future optoelectronic materials. In order to achieve this goal, material stability and point defect formation must be better understood and controlled. Our absorption and emission data strongly suggest that formation of defects and defect states are of importance in these materials. Nanocrystals are a good model system for studying the stability of double perovskite materials because of the ability to combine spectroscopy and observe structural changes with atomic resolution (HRTEM). We first study the stability of $Cs_2AgBiBr_6$ NCs in polar solvents, by conducting a series of experiments in which the NCs were suspended in solvents with increasing polar indices and the sharp absorption peak at 430 nm was monitored. As shown in Figure S7, $Cs_2AgBiBr_6$ NCs retain their spectroscopic properties in solvents with polar indices lower than 4.4 (ethyl acetate). Solvents with higher polarity index will induce degradation of the ionic nanocrystals and in some cases (dimethylformamide) a high energy peak at approximately 365 nm will form. A similar peak is assigned in the literature to a charged $BiBr_5^{2-}$ molecular complex, which may be one of the resulting species of $Cs_2AgBiBr_6$ NCs degradation.[36] A second stability study examined the reactions of nanocrystals with different ligand binding groups by monitoring the NCs optical properties. In this experiment the different ligands were introduced in excess (0.06%-3.6% weight/volume) to a colloidal suspension of NCs at room

temperature. Thiols and carboxylic acids did not evoke any clear spectral changes, while phosphonic acids suppressed the emission from the nanocrystals but kept the crystal absorption intact. The most important observation in this experiment was with excess primary and tertiary amines which caused significant spectral changes in the crystals, leading to a disappearance of absorption (and emission) features, which we interpret as complete dissolution of the NCs (see Figure S8 for complete list and spectra). This result may suggest a similar surface chemistry for the double perovskite nanocrystals to those of the lead halides in which oleylammonium plays an important role in passivating the halide atoms on the surface,[38] and excess amines degrade the NCs.[39]

Amines are reducing agents and can produce silver particles in the presence of silver ions. In TEM studies small circular nanoparticles are frequently observed as higher contrast decorations on the facets or inside the NCs. For reactions at high temperatures (200 ^{0}C) the size of these nanoparticles will increase with time. In 3 min reactions their average size is 2.4±0.7 nm, gradually increasing to 4.1±1.1 nm after 60 minutes. (Figure 4, S9) Longer reactions of 90 minutes result in many degraded $Cs_2AgBiBr_6$ NCs; higher contrast circular particles both attached to the $Cs_2AgBiBr_6$ NCs and in some cases separated from them are observed. This reaction time size dependence suggests that these higher contrast decorations are intrinsic to the crystal growth process and not an artifact of TEM imaging. To further understand the degradation pathway of $Cs_2AgBiBr_6$ NCs we conducted a

STEM-EDS study of NCs with these higher contrast decorations. (Figure 5a yellow and red areas respectively). Elemental analysis indicates that these small particles contain almost exclusively silver atoms, suggesting that they are silver nanocrystals (Figure 5b EDS mapping and Table 1 for details). In contrast, the cubic nanocrystals in the background contains stoichiometric amounts of Ag^{+} and Bi^{3+}, consistent with their assignment as $Cs_2AgBiBr_6$ material.

We also performed high resolution TEM structural analysis on higher contrast islands still attached to $Cs_2AgBiBr_6$ NCs. These small nanoparticles exhibit a distinct lattice fringe (Figure 5c) that does not overlap with those of the background perovskite material. Using selective Fourier filtering (Figure 5d,e,f), we measured a lattice spacing for the higher contrast island of 0.24 nm, which matches the <111> spacing of metallic silver. The background lattice spacing is 0.4 nm, similar to the double perovskite <022> spacing. The larger, Ag-depleted nanocrystals undergo a transition from the cubic Fm-3m $Cs_2AgBiBr_6$ to trigonal p-3m1 $Cs_3Bi_2Br_9$ and Cs_3BiBr_6 nanocrystals as confirmed spectroscopically and by XRD (Figure S8 a,b). The overall shape of these byproduct nanocrystals is no longer cubic and more rounded crystals or triangular prisms are observed (Figure S8 c,d). The degradation products we have observed are summarized in the following reaction equation,

$$3Cs_2AgBiBr_6 \rightarrow Cs_3Bi_2Br_9 + Cs_3BiBr_6 + 3Ag + \frac{3}{2}Br_2$$

Including the two different ternary $Cs_xBi_YBr_z$ compositions and elemental silver we have observed in optical measurements and in the transmission electron microscope. The oxidation of bromides to bromine is used here for simplification. It is likely that other species, such as oleylamine, would be oxidized first. These observations reveal a prominent degradation pathway of $Cs_2AgBiBr_6$ NCs, in which silver diffusion, reduction and coalescence are identified as the key source of structural instability.

Previous DFT studies have discussed the thermodynamic stability and degradation pathways of silver bismuth double perovskites. Formation enthalpy calculation shows that under carefully controlled chemical conditions the silver bismuth double perovskites are stable.[40] Regarding decomposition pathways, the formation of metallic silver can be thermodynamically favorable under bromine poor conditions, in agreement with our observations. Intuitively, due to the low standard reduction potential of silver, a reducing environment, for example the presence of amine ligands (discussed earlier) may additionally destabilize the perovskite structures by formation of metallic silver. Indeed, we observe that when not washed from excess ligands degradation processes occur and affect colloidal NCs that are in hexanes and ambient conditions. By removing the NCs from solution and forming solid NC films these degradation processes decrease. This was verified by comparing XRD patterns of fresh dry films and after 90 days of storage in ambient conditions. (Figure S11)

Since dry $Cs_2AgBiBr_6$ NC films are stable and potentially interesting for future applications, we studied the translational ordering in self-assembled NC superlattices. After carefully cleaning the NCs, superlattices were assembled by controlled evaporation rate of the solvents, inducing strong ligand-ligand interactions. The NCs were assembled in a quartz capillary (slow solvent evaporation) and on a silicon substrate (both slow and fast evaporation). The substrates were then characterized by SEM and measured by transmission and grazing-incidence small-angle X-ray scattering (SAXS and GISAXS). SEM images (Figure 6a) depict long range ordering of the nanocrystals into superlattices hundreds of nanometers in length. A GISAXS intensity map measured on the same sample (Figure 6b) demonstrates scattering peaks of ordered NCs both in plane and out-of-plane with respect to the substrate. In the integrated angular 1D data (Figure 6c), a main scattering peak at q values of 0.535 nm^{-1} and 0.52 nm^{-1} is observed for the GISAXS and transmission mode experiments respectively (Figure S12). These correspond to distances of 12±0.3 nm and 11.7±0.3 nm respectively reflecting the distance between the centers of scatterers, corresponding to the NC side length with the addition of capping ligands (chain length of oleic acid or oleylamine). The full width half maximum of these peaks is Δq=0.01 nm^{-1} and 0.07 nm^{-1}, with a sharper peak for the slowly dried quartz capillary sample indicating higher degree of ordering. Higher order scattering peaks with values of $\sqrt{2}q$ and $2q$ are also observed (Figure 6f dashed lines). These experiments further confirm the homogenous shape and size distribution of

the colloidal sample on a macroscopic scale, and the ordered nature of these solid NC films. The combination of stability and high order of the closed pack dry NC films is of great importance for future development of lead free perovskites into useful materials.

In conclusion, we study stability of lead free halide double perovskite nanocrystals with silver-bismuth compositions. The structural characterization matches that of recently reported bulk counterparts. A sharp peak at 430 nm for $Cs_2AgBiBr_6$ and 365 nm for $Cs_2AgBiCl_6$ dominates the absorption spectra of the nanocrystals. The peak, which is 1 eV higher in energy than the band edge, is identified as a localized Bi 6s-to-6p transition, not as a confined exciton. Utilizing advanced electron microscopy techniques combined with optical spectroscopy, we identify Ag diffusion and coalescence along with the formation of $Cs_3Bi_2Br_9$ and Cs_3BiBr_6 as a key degradation pathway in these nanocrystals. These degradation processes are significantly slower in dry NC solids. The lead-free, double perovskite nanocrystals can serve as a model system to further improve stability of these materials and to explore other lead free compositions with a more direct electronic transition that can serve future optoelectronic applications.

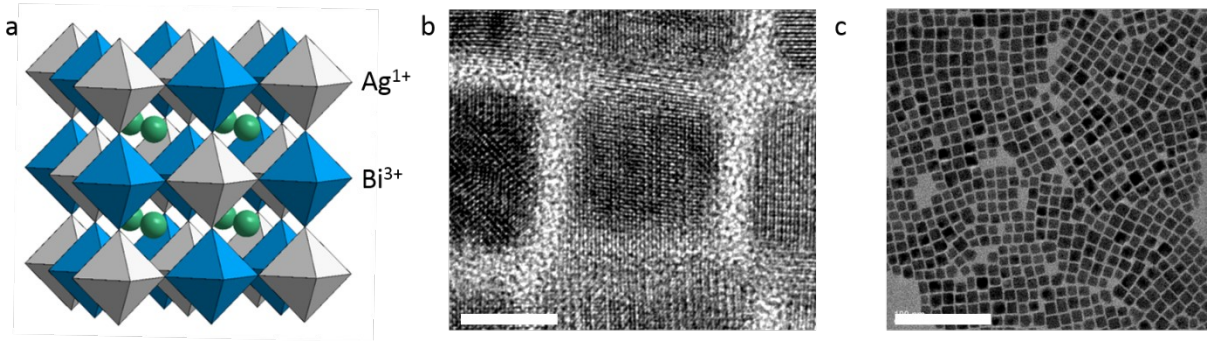

Figure 1. Morphological characterization of $Cs_2AgBiBr_6$ NCs. (a) Cartoon of the extended unit cell of lead free double perovskite; gray and blue depict the Ag (I) and Bi (III) octahedral respectively. Cs atoms are shown in green. (b) High resolution TEM image of $Cs_2AgBiBr_6$ NCs depicting atomic lattice fringes, and the faceted cubic shape of the crystals. The scale bar is 8 nm. (c) Low resolution TEM image of the same sample. The scale bar is 100 nm

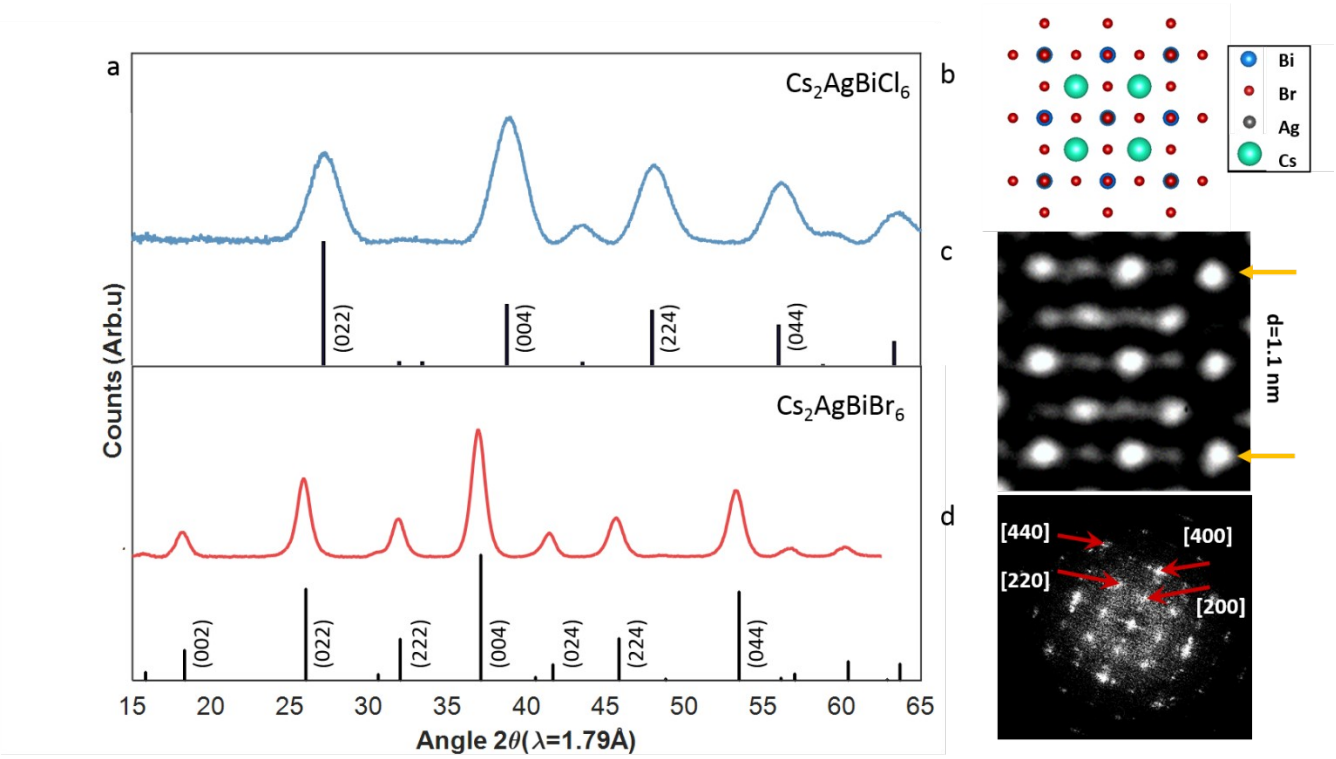

Figure 2. Structural Characterization. (a) XRD Patterns of $Cs_2AgBiBr_6$ (red) and $Cs_2AgBiCl_6$ (blue) NCs compared to reported pattern. (b) Model of an extended unit cell of $Cs_2AgBiBr_6$, viewed down the 100 zone axis. (c) HRTEM of a unit cell depicting a contrast difference between columns with Bi/Ag and Cs compared to those with only halides. The (001) lattice spacing is measured to be 1.1 nm (d) FFT analysis of lattice fringes from a few oriented NCs demonstrates the cubic nature of this crystal structure on the nanoscale.

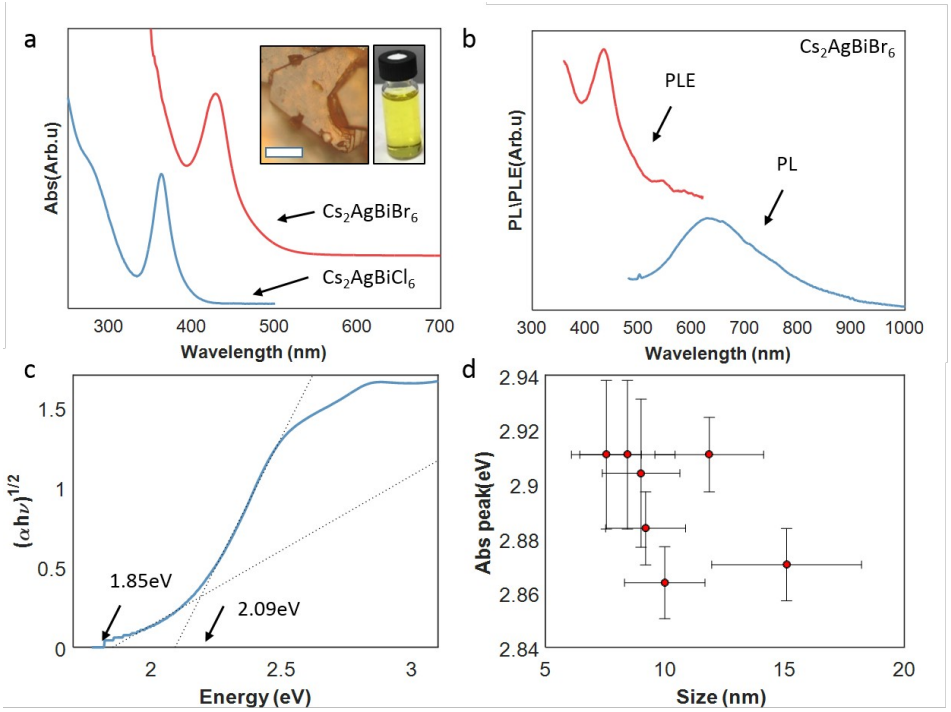

Figure 3. Optical properties of the $Cs_2AgBiBr_6$ NCs. (a) UV/VIS absorption of dilute $Cs_2AgBiBr_6$ (red) and $Cs_2AgBiCl_6$ (blue) NCs suspensions demonstrating the characteristic peaks at 430 nm and 365 nm, respectively. Inset showing a suspension of $Cs_2AgBiBr_6$ NCs, with distinct yellow color different from the orange-red bulk material. (b) Photoluminescence from excited $Cs_2AgBiBr_6$ NCs (blue) (λ_{exc} = 430 nm), which is similar to photoluminescence described in the literature for bulk crystals. Photoluminescence excitation scan collected at 650 nm (red) traces the absorption peak at 430 nm. (c) Tauc plot of diffuse absorption measurements of NC films assuming indirect band gap characteristics gives similar measurements of direct (2.09 eV) and indirect (1.85 eV) to that of bulk crystals. (d) A plot of center of absorption peak vs smallest side length of cubes shows no strong dependence of the absorption

peak on size, which rules out quantum confinement as a strong contribution to the high energy position of this peak.

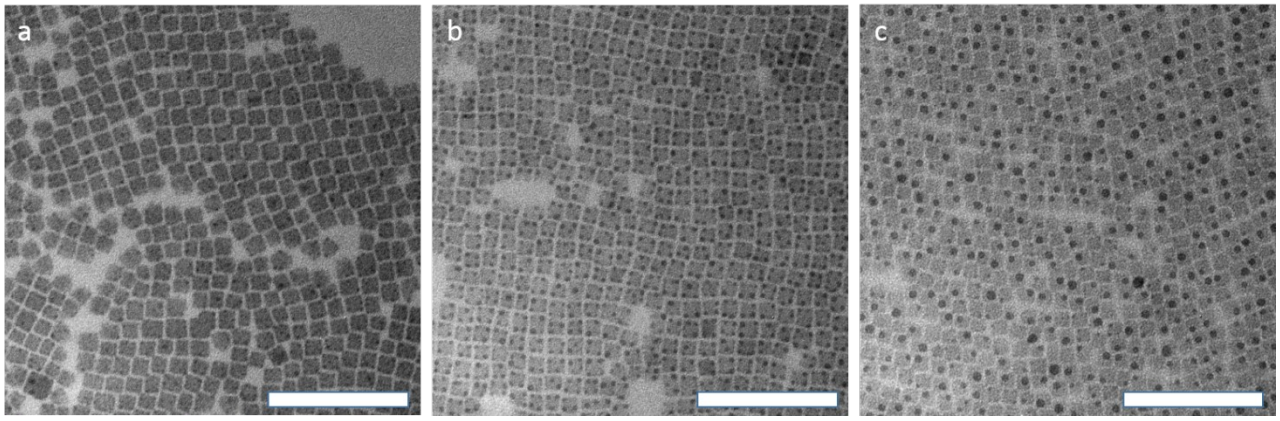

Figure 4. Size evolution of particles decorating $Cs_2AgBiBr_6$ NCs. TEM images depicting cubic $Cs_2AgBiBr_6$ NCs and circular, high-contrast particles decorating the cubes. After (a) 10 min (b) 30 min (c) 60 min of crystal growth reaction. The scale bar is 100 nm.

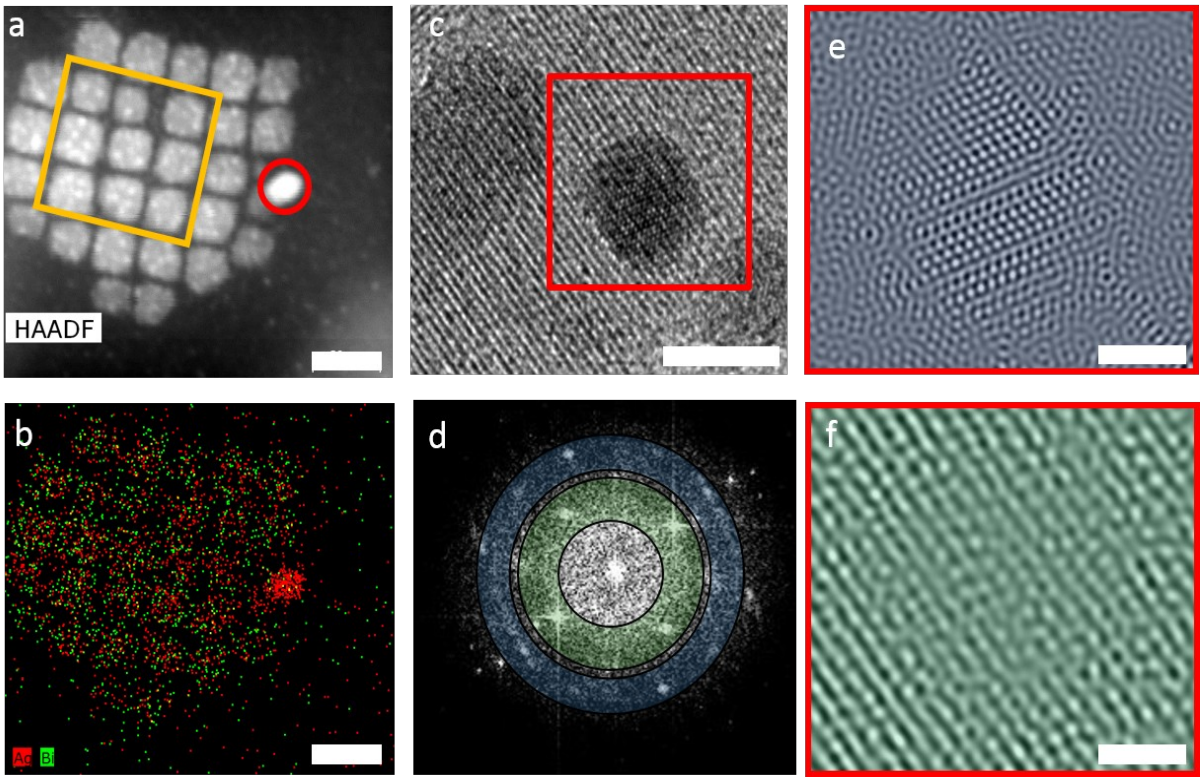

Figure 5. Degradation of $Cs_2AgBiBr_6$. (a) HAADF image depicting cubic $Cs_2AgBiBr_6$ NCs and a circular, high-contrast particle. The bright decorations on the cubic NCs are assigned to silver islands. STEM-EDS analysis is used to compare the composition of the yellow frame and red circle areas (Table 1), the scale bar is 20 nm. (b) STEM-EDS images showcasing the uniform distribution of silver and bismuth co-localized in the cubic nanocrystals. The bright circular particle (red) is a silver NC, the scale bar is 20 nm. (c) HRTEM of the decorations on cubic $Cs_2AgBiCl_6$ crystals showing lattice spacing for both the silver nanoparticle and the underlying double perovskite crystal, the scale bar is 2 nm. (d) FFT of the selected area in panel c (red) depicting two

different periodicities marked in blue and green. By Fourier filtering the different components, a lattice spacing of (e) 0.24 nm that matches (111) of silver (blue) and (f) 0.4 nm that matched the double perovskites (220) (green) can be clearly separated, the scale bar is 1 nm.

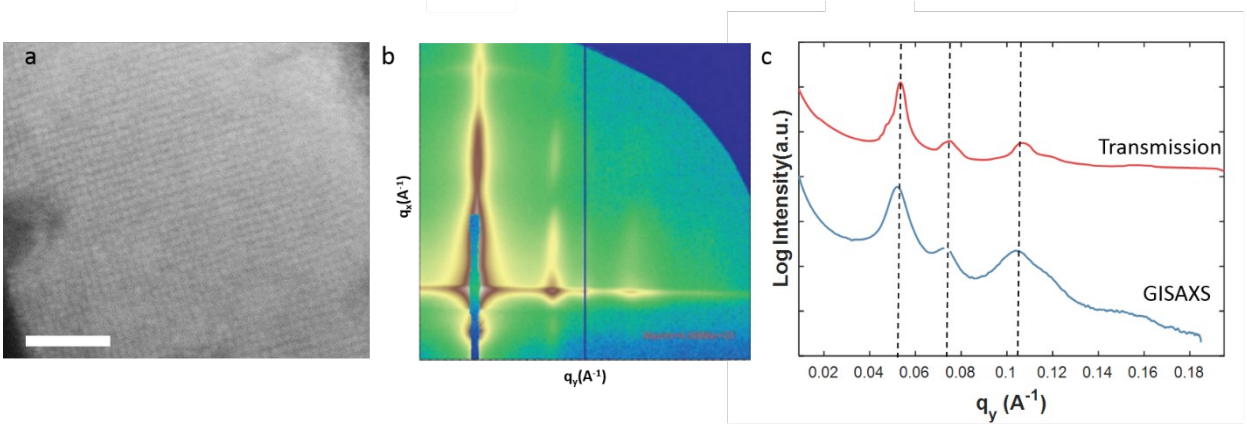

Figure 6. Characterization of $Cs_2AgBiBr_6$ NCs solids. (a) SEM image of $Cs_2AgBiBr_6$ NCs self-assembled into super lattices on a Si substrate. The scale bar is 100 nm. (b) Grazing incidence-SAXS intensity map of $Cs_2AgBiBr_6$ NC superlattices. (c) Radially Integrated intensity of the scattering map illustrating the ordering of assemblies formed by slow evaporation in a quartz capillary (red) measured in transmission mode (intensity map in S12) and fast evaporation on a silicon substrate (blue) measured in GISAXS mode.

Table 1. STEM-EDS analysis Figure 5a

	9 cubic crystals (yellow)	**spherical nanocrystal (red)**

Element	Atom [%]	Std [%]	Atom [%]	Std [%]
Cs	24.9	3.2	1.1	1
Ag	13.4	1.5	92.5	11.4
Bi	11.7	2.5	1.6	1.8
Br	50.0	1.6	4.9	1.5

ASSOCIATED CONTENT

Supporting Information. Experimental details, calculations, and additional figures including TEM, XRD, SEM, EDS, and PL data.

AUTHOR INFORMATION

Corresponding Author

*Email: apalivisatos@berkeley.edu

Author Contributions

The manuscript was written through contributions of all authors. All authors have given approval to the final version of the manuscript.

Notes

The authors declare no competing financial interest.

ACKNOWLEDGMENT

This work was supported by the U.S. Department of Energy, Office of Science, Office of Basic Energy Sciences, Materials Sciences and Engineering Division, under Contract No. DE-AC02-05-CH11231 within

the Physical Chemistry of Inorganic Nanostructures Program (KC3103). Work at the Molecular Foundry was supported by the Office of Science, Office of Basic Energy Sciences, of the U.S. Department of Energy under Contract No. DE-AC02-05CH11231. Y.B acknowledges support from the Sackler Fellowship. J.D acknowledges support by the National Science Foundation Graduate Research Fellowship under DGE 1752814. The authors acknowledge Prof. Xun Wendy Gu for help with the GISAXS experiments and Yao Cai, Dr. Assaf Ben Moshe and Dr. Ayelet Teitelboim for fruitful discussion.

(1) Zhou, H.; Chen, Q.; Li, G.; Luo, S.; Song, T. -b.; Duan, H.-S.; Hong, Z.; You, J.; Liu, Y.; Yang, Y. *Science.* **2014**, *345*, 542–546.

(2) Burschka, J.; Pellet, N.; Moon, S.-J.; Humphry-Baker, R.; Gao, P.; Nazeeruddin, M. K.; Grätzel, M. *Nature* **2013**, *499*, 316–319.

(3) Lee, M. M.; Teuscher, J.; Miyasaka, T.; Murakami, T. N.; Snaith, H. J. *Science* **2012**, *338* , 643–647.

(4) Eaton, S. W.; Lai, M.; Gibson, N. A.; Wong, A. B.; Dou, L.; Ma, J.; Wang, L.-W.; Leone, S. R.; Yang, P. *Proc. Natl. Acad. Sci.* **2016**, *113*, 1993–1998.

(5) Dou, L.; Yang, Y. (Micheal); You, J.; Hong, Z.; Chang, W.-H.; Li, G.; Yang, Y. *Nat. Commun.* **2014**, *5*, 5404.

(6) Tan, Z.-K.; Moghaddam, R. S.; Lai, M. L.; Docampo, P.; Higler, R.; Deschler, F.; Price, M.; Sadhanala, A.; Pazos, L. M.; Credgington, D.; Hanusch, F.; Bein, T.; Snaith, H. J.; Friend, R. H. *Nat. Nanotechnol.* **2014**, *9*, 687–692.

(7) Nagabhushana, G. P.; Shivaramaiah, R.; Navrotsky, A. *Proc. Natl. Acad. Sci.* **2016**, *113* , 7717–7721.

(8) Hailegnaw, B.; Kirmayer, S.; Edri, E.; Hodes, G.; Cahen, D. *J. Phys. Chem. Lett.* **2015**, *6*, 1543–1547.

(9) Goldschmidt, V. M. *Naturwissenschaften* **1926**, *14*, 477–485.

(10) Pauling, L. *J. Am. Chem. Soc.* **1929**, *51*, 1010–1026.

(11) Travis, W.; Glover, E. N. K.; Bronstein, H.; Scanlon, D. O.; Palgrave, R. G. *Chem. Sci.* **2016**, *7*, 4548–4556.

(12) Hao, F.; Stoumpos, C. C.; Cao, D. H.; Chang, R. P. H.; Kanatzidis, M. G. *Nat. Photonics* **2014**, *8*, 489–494.

(13) Noel, N. K.; Stranks, S. D.; Abate, A.; Wehrenfennig, C.; Guarnera, S.; Haghighirad, A.-A.; Sadhanala, A.; Eperon, G. E.; Pathak, S. K.; Johnston, M. B.; Petrozza, A.; Herz, L. M.; Snaith, H. J. *Energy Environ. Sci.* **2014**, *7*, 3061–3068.

(14) Chung, I.; Song, J.-H.; Im, J.; Androulakis, J.; Malliakas, C. D.; Li, H.; Freeman, A. J.; Kenney, J. T.; Kanatzidis, M. G. *J. Am. Chem. Soc.* **2012**, *134*, 8579–8587.

(15) Wang, A.; Yan, X.; Zhang, M.; Sun, S.; Yang, M.; Shen, W.; Pan, X.; Wang, P.; Deng, Z. *Chem. Mater.* **2016**, *28*, 8132–8140.

(16) Saparov, B.; Hong, F.; Sun, J.-P.; Duan, H.-S.; Meng, W.; Cameron, S.;

Hill, I. G.; Yan, Y.; Mitzi, D. B. *Chem. Mater.* **2015**, *27*, 5622–5632.

(17) Cortecchia, D.; Dewi, H. A.; Yin, J.; Bruno, A.; Chen, S.; Baikie, T.; Boix, P. P.; Grätzel, M.; Mhaisalkar, S.; Soci, C.; Mathews, N. *Inorg. Chem.* **2016**, *55*, 1044–1052.

(18) Pal, J.; Manna, S.; Mondal, A.; Das, S.; Adarsh, K. V.; Nag, A. *Angew. Chemie Int. Ed.* **2017**, *56*, 14187–14191.

(19) Slavney, A. H.; Hu, T.; Lindenberg, A. M.; Karunadasa, H. I. *J. Am. Chem. Soc.* **2016**, *138*, 2138–2141.

(20) McClure, E. T.; Ball, M. R.; Windl, W.; Woodward, P. M. *Chem. Mater.* **2016**, *28*, 1348–1354.

(21) Volonakis, G.; Filip, M. R.; Haghighirad, A. A.; Sakai, N.; Wenger, B.; Snaith, H. J.; Giustino, F. *J. Phys. Chem. Lett.* **2016**, *7*, 1254–1259.

(22) Tran, T. T.; Panella, J. R.; Chamorro, J. R.; Morey, J. R.; McQueen, T. M. *Mater. Horiz.* **2017**, *4*, 688–693.

(23) Zhao, X.-G.; Yang, D.; Sun, Y.; Li, T.; Zhang, L.; Yu, L.; Zunger, A. *J. Am. Chem. Soc.* **2017**, *139*, 6718–6725.

(24) Slavney, A. H.; Leppert, L.; Bartesaghi, D.; Gold-Parker, A.; Toney, M. F.; Savenije, T. J.; Neaton, J. B.; Karunadasa, H. I. *J. Am. Chem. Soc.* **2017**, *139*, 5015–5018.

(25) Du, K.; Meng, W.; Wang, X.; Yan, Y.; Mitzi, D. B. *Angew. Chemie Int. Ed.* **2017**, *56*, 8158–8162.

(26) Swarnkar, A.; Ravi, V. K.; Nag, A. *ACS Energy Lett.* **2017**, *2*, 1089–1098.

(27) Creutz, S. E.; Crites, E. N.; De Siena, M. C.; Gamelin, D. R. *Nano Lett.* **2018**, *18*, 1118–1123.

(28) Protesescu, L.; Yakunin, S.; Bodnarchuk, M. I.; Krieg, F.; Caputo, R.; Hendon, C. H.; Yang, R. X.; Walsh, A.; Kovalenko, M. V. *Nano Lett.* **2015**, *15*, 3692–3696.

(29) Xu, K.; Lin, C. C.; Xie, X.; Meijerink, A. *Chem. Mater.* **2017**, *29*, 4265–4272.

(30) Bekenstein, Y.; Koscher, B. A.; Eaton, S. W.; Yang, P.; Alivisatos, A. P. *J. Am. Chem. Soc.* **2015**, *137*, 16008–16011.

(31) Sichert, J. A.; Tong, Y.; Mutz, N.; Vollmer, M.; Fischer, S.; Milowska, K. Z.; García Cortadella, R.; Nickel, B.; Cardenas-Daw, C.; Stolarczyk, J. K.; Urban, A. S.; Feldmann, J. *Nano Lett.* **2015**, *15*, 6521–6527.

(32) Weidman, M. C.; Goodman, A. J.; Tisdale, W. A. *Chem. Mater.* **2017**, *29*, 5019–5030.

(33) Connor, B. A.; Leppert, L.; Smith, M. D.; Neaton, J. B.; Karunadasa, H. I. *J. Am. Chem. Soc.* **2018**, *140*, 5235–5240.

(34) Leng, M.; Chen, Z.; Yang, Y.; Li, Z.; Zeng, K.; Li, K.; Niu, G.; He, Y.; Zhou, Q.; Tang, J. *Angew. Chemie Int. Ed.* **2016**, *55*, 15012–15016.

(35) Yang, B.; Chen, J.; Hong, F.; Mao, X.; Zheng, K.; Yang, S.; Li, Y.; Pullerits, T.; Deng, W.; Han, K. *Angew. Chemie Int. Ed.* **2017**, *56*, 12471–12475.

(36) Oldenburg, K.; Vogler, A. **1993**, *48*, 1519–1523.

(37) Pan, W.; Wu, H.; Luo, J.; Deng, Z.; Ge, C.; Chen, C.; Jiang, X.; Yin, W.-J.; Niu, G.; Zhu, L.; Yin, L.; Zhou, Y.; Xie, Q.; Ke, X.; Sui, M.; Tang, J. *Nat. Photonics* **2017**, *11*, 726–732.

(38) De Roo, J.; Ibáñez, M.; Geiregat, P.; Nedelcu, G.; Walravens, W.; Maes, J.; Martins, J. C.; Van Driessche, I.; Kovalenko, M. V; Hens, Z. *ACS Nano* **2016**, *10*, 2071–2081.

(39) Liu, Z.; Bekenstein, Y.; Ye, X.; Nguyen, S. C.; Swabeck, J.; Zhang, D.; Lee, S.-T.; Yang, P.; Ma, W.; Alivisatos, A. P. *J. Am. Chem. Soc.* **2017**, *139*, 5309–5312.

(40) Xiao, Z.; Meng, W.; Wang, J.; Yan, Y. *ChemSusChem* **2016**, *9*, 2628–2633.

TOC: